Electronic characterization of polar nanoregions in relaxor-type ferroelectric $NaNbO_3$ films

Biya Cai,[1] J. Schwarzkopf,[2] E. Hollmann,[1] D. Braun,[2] M. Schmidbauer,[2] T. Grellmann,[1] and R. Wördenweber[1]
[1]*Peter Grünberg Institute (PGI) and JARA-Fundamentals of Future Information Technology, Forschungszentrum Jülich, D-52425 Jülich, Germany*
[2]*Leibniz Institute for Crystal Growth, Max-Born-Straße 2, D-12489 Berlin, Germany*
(Received 13 October 2015; revised manuscript received 22 April 2016; published 22 June 2016)

Strained $NaNbO_3$ films of different thicknesses are epitaxially grown on (110) $NdGaO_3$ substrates. A detailed analysis of the permittivity of these films demonstrates that strain not only leads to a modification of the permittivity and the ferroelectric transition temperature, it also results in a pronounced relaxor-type behavior and allows a direct estimation of the size and mobility of the polar nanoregions (PNRs). The compressive strain reduces the transition temperature to 125 K and enhances the corresponding permittivity up to $\varepsilon' \approx 1500$ for the thinnest film. Since the strain relaxes with increasing film thickness, both effects, reduction of phase transition temperature and enhancement of ε', depend on the thickness of the film. The films show a characteristic frequency and electric field dependence of ε', which is discussed in terms of the Vogel-Fulcher equation and Rayleigh law, respectively. Using the electric field dependence of the resulting freezing temperature T_{VF}, allows a direct estimation of the volume of the PNRs at the freezing temperature, i.e. from 70 to 270 nm^3. Assuming an idealized spherical shape of the PNRs, diameters of a few nanometers (5.2–8 nm) are determined that depend on the applied ac electric field. The irreversible part of the polarization seems to be dominated by the presence and mobility of the PNRs. It shows a characteristic peak at low temperature around T_{VF}, vanishes at a temperature where the activation energy of the PRNs extrapolates to zero, and shows a frequency dispersion that is characteristic for relaxor-type behavior.

DOI: 10.1103/PhysRevB.93.224107

I. INTRODUCTION

Relaxor-type ferroelectrics recently attracted considerable scientific interest owing to their intriguing physics and their potentially high permittivity and tunability, resulting in a number of potential applications [1]. Generally relaxor-type ferroelectrics are characterized by their frequency-dependent and broad peak in the temperature dependence of the permittivity that is believed to be based on the formation of regions of uniform polarization, the so-called polar nanoregions (PNRs) [2]. In classical relaxor-type ferroelectrics, such as lanthanum-doped lead zirconate titanate (PLZT) or lead magnesium niobate (PMN), it is assumed that secondary phases or inhomogeneities (chemical or structural) might be responsible for the formation of the PNRs [3–6]. As a consequence, the size of the PNRs is usually assumed to be associated with the extension of these secondary phases or inhomogeneities. The existence of both the polar cluster and the matrix into which the polar clusters are embedded in the relaxor-type state was demonstrated, for instance, by neutron scattering, nuclear magnetic resonance (NMR), and x-ray diffraction experiments [5,7–10]. Whereas, for the interaction of the PNRs, two major models are accepted [6,11], i.e. a dipole-glass model [12–16] and a random-field model [17,18], the size of the PNR is still discussed controversially.

Direct observation of the local polarization using piezoresponse-force microscopy (PFM) suggests rather extended regions of uniform polarization of up to a few hundred nanometers in diameter [19]; neutron scattering measurements indicate the length scale of the PNRs is several nanometers [5,7]; and transmission electron microscope (TEM) images show local variations of the structure and thus uniform polarization of a size of 10 to 20 nm [6] or even only a few unit cells [20] that could be associated with the PNRs. The latter is supported by simulation [21]. However, PFM as well as TEM observations are mainly restricted to surface properties, whereas PNRs are expected to exist in the bulk, i.e. three-dimensional (3D) polar clusters embedded in a dielectric or ferroelectric matrix. Furthermore, all techniques refer to static polarization, whereas in electronic (i.e. frequency-dependent) measurements, the mobility of the PNRs plays a major role. Therefore, a direct measurement of the size and mobility of the PNRs would be desirable.

In this paper, we analyze the size and mobility of PNRs in compressively strained $NaNbO_3$ thin films. Generally, $NaNbO_3$-based materials have attracted significant scientific and technological interest due to their complexity of phase transitions [22–24], excellent ferro-/piezoelectric properties, and their highly interesting electric behavior [25]. Lately, it has been shown that strain cannot only be used to very effectively engineer ferroelectric properties (e.g. shift the transition temperature and enhance the permittivity significantly), it can also result in prominent relaxor behavior of material that shows classical ferroelectric behaviors in the unstrained state [26,27]. Most likely, the strain leads to a minute deviation from the perfect stoichiometry, resulting in the formation of PNRs [28]. Recently, we demonstrated that $NaNbO_3$ epitaxially grown on lattice-mismatched substrate shows such a behavior [25,29]. Here, we discuss the impact of strain relaxation on the ferroelectric properties by analyzing films of different thickness and investigating the frequency and electric field (ac and dc) dependence of the permittivity. Via our experiments, we are able to directly evaluate the size of the PNRs from our electronic measurements and demonstrate that PNRs significantly attribute to irreversible contribution to the permittivity.

II. SAMPLE PREPARATION AND EXPERIMENTAL TECHNIQUES

$NaNbO_3$ films are deposited via liquid-delivery spin metal-organic chemical vapor deposition (MOCVD) at a temperature of 700 °C on (110) oriented single-crystalline $NdGaO_3$

 ©2016 American Physical Society

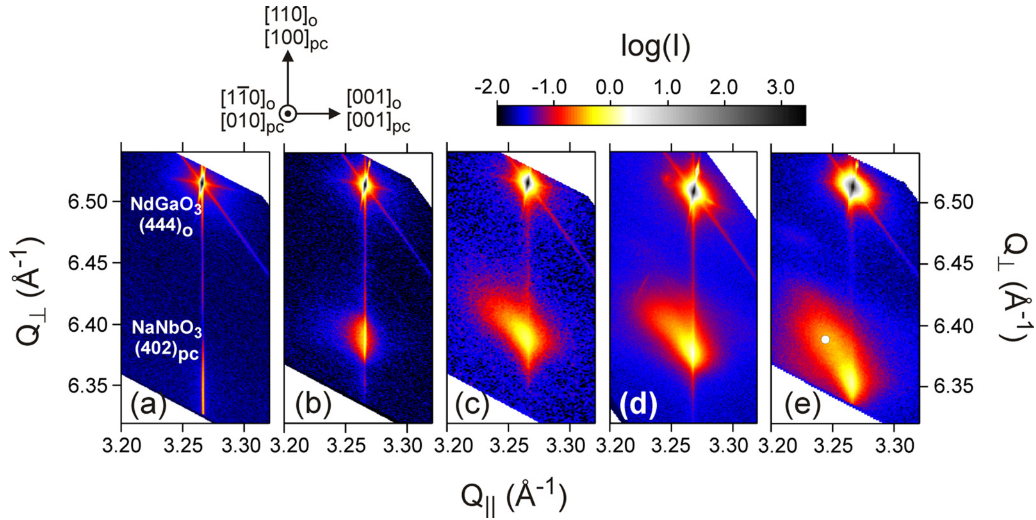

FIG. 1. High-resolution x-ray diffraction RSM in the vicinity of the $(444)_o$ Bragg reflection of the $NdGaO_3$ substrate for (a) 11-, (b) 27-, (c) 63-, (d) 80-, and (e) 140-nm-thick samples. The circle in (e) marks the position of the corresponding $(402)_{pc}$ reflection of unstrained $NaNbO_3$.

substrates. The $NdGaO_3$ substrates are slightly off-oriented (0.1°) and annealed in pure oxygen flow at 1050 °C for 1 h. This generates a regular step-and-terrace surface structure with NdO surface termination [30] and promotes step flow growth of the $NaNbO_3$ film. A detailed description of the MOCVD deposition technique and the deposition parameters are given in Ref. [31].

From the orthorhombic lattice parameters of bulk $NaNbO_3$, the corresponding pseudocubic values according to Vailionis *et al.* [32] are $a_{pc} = 3.881$ Å, $b_{pc} = c_{pc} = 3.915$ Å, and $\alpha = 89.33°$. The substrate's surface, (110) $NaGaO_3$, exhibits a nearly squared in-plane lattice with lattice parameters of 2×3.863 and 2×3.854 Å in $[110]_o$ and $[001]_o$ direction, respectively. In the further course of this paper, we will use the index *pc* for the pseudocubic system of the film, respectively, while the index *o* refers to the orthorhombic lattice of the $NdGaO_3$ substrate. The most probable film orientation can be estimated by considering the elastic strain energy density in the films incorporated by the epitaxial growth of $NaNbO_3$ on the lattice mismatched $NdGaO_3$ substrate. Two different main film orientations, $(100)_{pc}$ and $(001)_{pc}$, as well as a 90° rotated in-plane variant for $(001)_{pc}$-oriented films have to be considered, resulting in three different configurations. The lowest elastic strain energy density is obtained for $(001)_{pc}$ surface orientation of the film and the in-plane epitaxial relationship $[010]_{pc} \parallel [110]_o$ and $[100]_{pc} \parallel [001]_o$. Thus, we expect that the films grow with $(001)_{pc}$ surface orientation under compressive in-plane strain with resulting nominal lattice mismatches of 1.35 and 0.70% in $[110]_o$ and $[001]_o$, respectively.

The structural properties of the $NaNbO_3$ films are analyzed via high-resolution x-ray diffraction experiments [31]. Reciprocal space maps (RSMs) in the vicinity of the asymmetric $(444)_o$ Bragg reflection of the orthorhombic $NdGaO_3$ substrate on $NaNbO_3$ films of different thicknesses are shown in Fig. 1. All RSM patterns prove the epitaxial growth of the films, i.e. the in-plane component of the scattering vectors of the $(444)_o$ Bragg reflection $Q_\parallel$ of $NdGaO_3$ and of the main intensity of the $(402)_{pc}$ Bragg reflection of the $NaNbO_3$ films coincide. However, for the 27-nm-thick film, the $(402)_{pc}$ reflection peak of the film broadens asymmetrically to the left side [Fig. 1(b)], and with further increasing film thickness, the film contribution expands towards lower $Q_\parallel$ values, i.e. larger in-plane lattice parameters [Figs. 1(c)–1(e)]. This is clearly noticeable for the 140 nm film in Fig. 1(e), where the film reflection peak spreads towards the corresponding reciprocal lattice point of unstrained $NaNbO_3$ marked by the white circle. This observation is an indication for a partial plastic relaxation of the strained lattice of the film. This process starts at a critical thickness of 15–20 nm [31] and becomes more prominent with increasing thickness. Nevertheless, even for the thickest film (140 nm), the main intensity of the $(402)_{pc}$ reflection of the film is still at $Q_\parallel$ of the substrates; however, noticeable intensity is detected nearby the value of unstrained $NaNbO_3$, which is marked by a circle in Fig. 1(e).

For the investigation of the in-plane dielectric properties of the $NaNbO_3$ films, planar capacitors based on interdigitated electrodes (IDE) are employed. The IDEs are prepared via liftoff lithography technique and deposition of a thin (30 nm) Pt layer [27]. Since we do not consider the anisotropy of the lattice strain of the two orthogonal in-plane directions (for this see Ref. [29]) in this paper, only IDEs for the electric field oriented along the crystallographic direction with the smaller lattice parameter are considered, i.e. $E \parallel [001]NdGaO_3 \parallel [100]NaNbO_3$. It should be noted that the results of the other crystallographic direction ($E \parallel [110]NdGaO_3 \parallel [010]NaNbO_3$) are qualitatively identical. The ferroelectric properties are analyzed as function of temperature (20 to 400 K), frequency (20 Hz to 2 MHz), ac electric field (0.2 to 5 V), and dc bias (−5 to 5 V). The in-plane real part of the dielectric constant ε' of the $NaNbO_3$ films is calculated using the partial capacitance model [33–35].

III. EXPERIMENTAL RESULTS AND DISCUSSION

Generally, the temperature dependence of the permittivity ε' of the compressively strained $NaNbO_3$ films (Fig. 2) shows a distinct and broad peak at low temperature, which is indicative

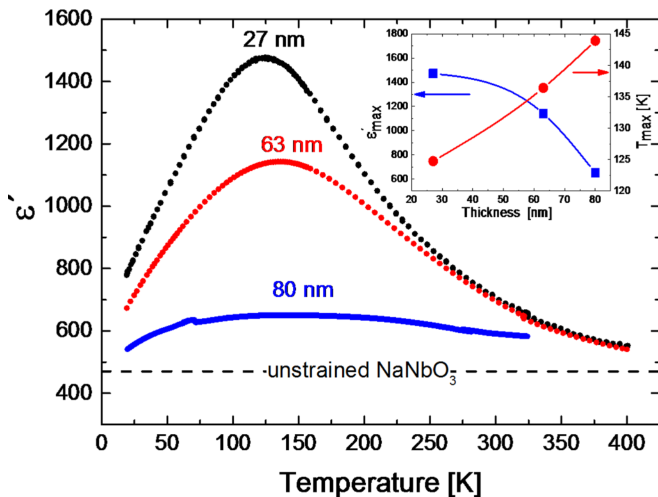

FIG. 2. Temperature dependence of the permittivity of $NaNbO_3$ films of different thicknesses that are epitaxially grown on (110) $NdGaO_3$. The data are recorded at 1 MHz using a small ac amplitude of $E_{ac} = 0.048\ \mathrm{V}\ \mu\mathrm{m}^{-1}$ and zero dc bias ($E_{dc} = 0$). The dash line represents the level of the dielectric constant of unstrained $NaNbO_3$ bulk material [36]. The inset shows the maximum dielectric constant ε'_{max} (blue squares) and the corresponding temperature T_{max} (red circles) as function of film thickness.

of a phase transition from a relaxor-type ferroelectric at low temperature to the dielectric state at high temperature [25,29]. The temperature of maximum permittivity T_{max} can be used as a first approximation of the temperature of the phase transition from the ferroelectric-to-dielectric phase transition. The compressive strain induced by the lattice parameter mismatch between the epitaxially grown film and the substrate leads to (i) a reduction of the temperature of maximum permittivity from that of unstrained bulk $NaNbO_3$ at $T_{max} \approx 628\ \mathrm{K}$ [36] to temperatures of $T_{max} = 125-147\ \mathrm{K}$ for the films of thicknesses ranging from 27 to 80 nm, and (ii) an enhancement of the permittivity up to 1500 at T_{max} in comparison to $\varepsilon'(T < 400\ \mathrm{K}) \approx 500$ of unstrained bulk material [36]. However, both effects strongly depend on the thickness of the $NaNbO_3$ film (see inset of Fig. 2). With increasing thickness, the maximum permittivity ε'_{max} decreases, whereas T_{max} increases. Both effects can be explained by the partial relaxation of the lattice strain in the film that was demonstrated by RSM measurements (see Fig. 1). The largest strain is present in the thinnest film, which possesses the lowest $T_{max} \approx 125\ \mathrm{K}$ and the largest $\varepsilon'_{max} \approx 1500$. With increasing thickness, partial plastic lattice relaxation sets in. As a consequence, the reduction of transition temperature becomes smaller, i.e. T_{max} increases. Moreover, the distribution of the strain (i.e. completely strained bottom layer relaxes toward the film surface) increases with increasing thickness. This leads to a broadening of the peak and thus a decrease of ε'_{max} with increasing thickness. Already at a thickness of 80 nm, the strain leads only to a relatively small enhancement of the permittivity of $\varepsilon'_{max} \approx 650$. This is not only caused by the progressive relaxation of the film, it is additionally enforced by the arrangement of the measurement. The planar set of IDEs predominantly records the permittivity of the top layer of the film, which represents the more relaxed part of the film. Therefore, and because the features that are discussed below are more pronounced for the thinner films, we will restrict our discussion to the measurement of the films with thickness of 27 nm and 63 nm, respectively.

Particularly the impact of the frequency and the electric field on the permittivity provides further insight to the ferroelectric properties of the strained films. Figure 3 summarizes the electric field dependence of the permittivity for the 27 and 63 nm thick $NaNbO_3$ films. It shows the change of the

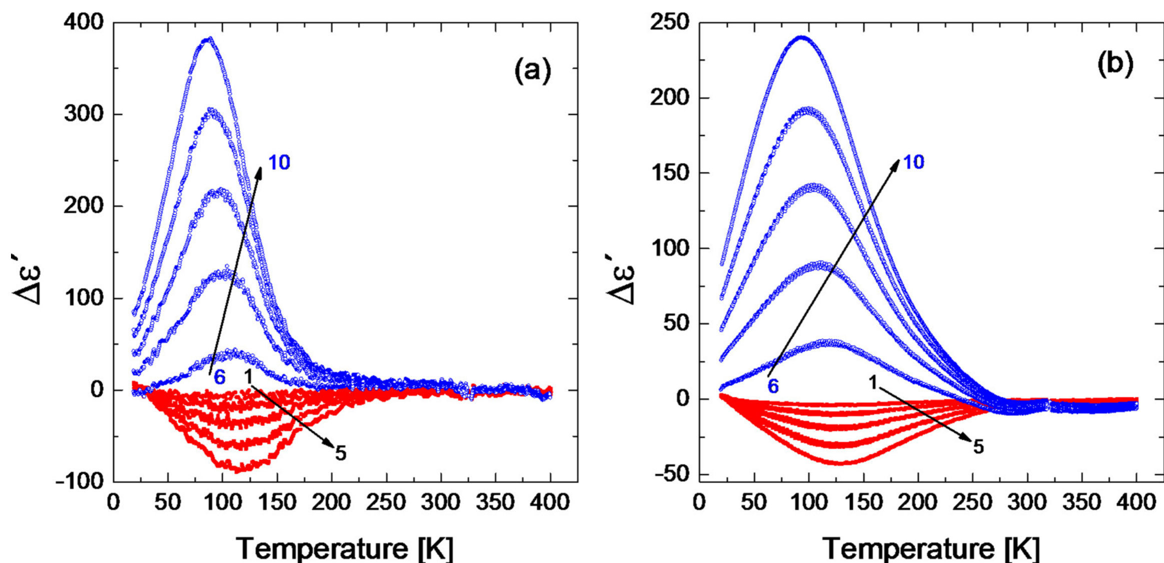

FIG. 3. Temperature dependence of the electric field-induced modification of the permittivity with respect to the data shown in Fig. 2 for the (a) 27- and (b) 63-nm-thick $NaNbO_3$ films, where $\Delta\varepsilon'$ is defined as $\Delta\varepsilon' = \varepsilon'(E_{ac}, E_{dc}) - \varepsilon'(E_{ac} = 0.048\ \mathrm{V}\ \mu\mathrm{m}^{-1}, E_{dc} = 0)$. For curves 1–5 (red solid symbols), the dc bias is varied from $E_{dc} = 0.2$ to $1\ \mathrm{V}\ \mu\mathrm{m}^{-1}$ in steps of $0.2\ \mathrm{V}\ \mu\mathrm{m}^{-1}$, and the ac field is kept at the minimum value of $E_{ac} = 0.048\ \mathrm{V}\ \mu\mathrm{m}^{-1}$; while for curves 6–10 (blue open symbols), the ac field amplitude is increased in steps of $0.2\ \mathrm{V}\ \mu\mathrm{m}^{-1}$ from $E_{ac} = 0.2$ to $1\ \mathrm{V}\ \mu\mathrm{m}^{-1}$ with $E_{dc} = 0$. The frequency is 1 MHz for all measurements; the arrows indicate the direction of increasing electric field.

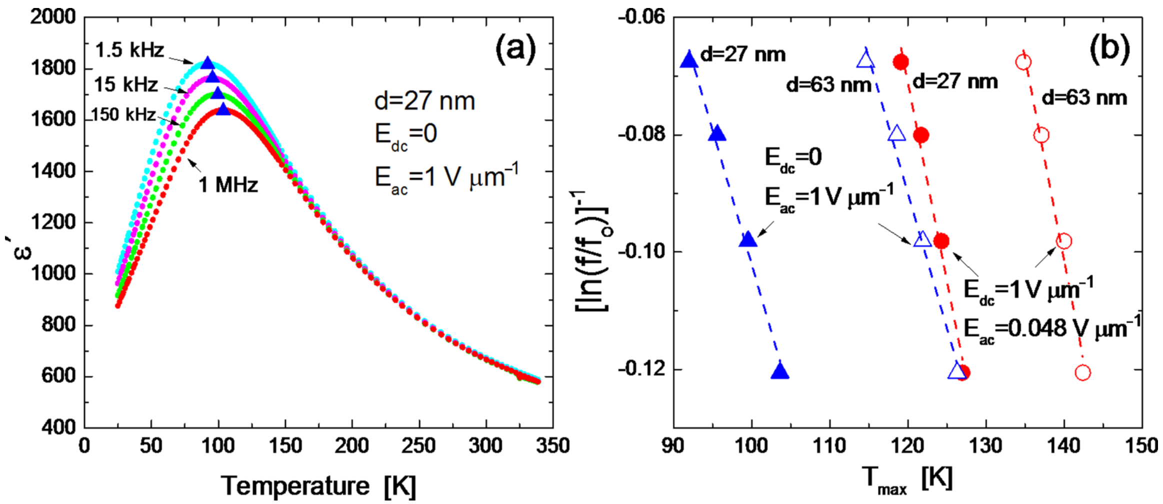

FIG. 4. Typical examples for (a) the frequency-dependent measurement of the permittivity (the position $T_{\max}$ is marked by blue triangles) and (b) the resulting Vogel-Fulcher fits (dash lines) based on Eq. (1) with $f_o = 4\,\text{GHz}$ for different electric field configurations for the 27 nm (solid symbols) and 63 nm (open symbols) thick films. The electric field values and thickness of the films are given in the figure.

permittivity $\Delta\varepsilon'$ with respect to the data recorded for the smallest electric field ($E_{\text{dc}} = 0$ and $E_{\text{ac}} = 0.048\,\text{V}\,\mu\text{m}^{-1}$) that are shown in Fig. 2. The impact of a dc bias is given in curves 1–5, which are measured for dc voltage of 1 to 5 V, respectively. In the paraelectric regime (i.e. the temperature regime close to the dielectric-to-ferroelectric transition temperature), a significant dc bias-dependent reduction of ε' is observed. The peak position hardly depends on the applied dc field. The paraelectric regime extends from approximately 25 to 250 K with a maximum tunability $n = \Delta\varepsilon'/\varepsilon'$ for only 5 V (equivalent to $1\,\text{V}\,\mu\text{m}^{-1}$) of $n \approx 7\%$ and $n \approx 3.8\%$ for the 27- and 63-nm-thick samples, respectively. This dc bias dependence agrees with that of classical ferroelectrics [37].

In contrast, an increase of the ac electric field leads to a pronounced increase of the permittivity in the paraelectric regime (see curves 6–10 in Fig. 3). Although the electric field strengths are identical to that of the dc bias (i.e. a maximum electric field of $1\,\text{V}\,\mu\text{m}^{-1}$ is applied in both cases) the impact of the ac field is several times (~6) larger than that of the dc bias. Furthermore, the position of the peak in the $\Delta\varepsilon'$ versus T plot depends on the ac field. Let us first discuss this behavior in the context of the frequency dependence of the permittivity. A detailed discussion of the ac field dependence will follow later.

Generally, the frequency dependence of the permittivity can serve as a fingerprint for relaxor-type ferroelectrics. In previous papers [25,29], we demonstrated that our compressively strained $NaNbO_3$ represents a relaxor-type ferroelectric. This is evident from the frequency-dependent shift of $T_{\max}$ according to the Vogel-Fulcher equation [38]

$$f = f_o \exp\left[-\frac{E_a}{k_{\text{B}}(T_{\max} - T_{\text{VF}})}\right], \tag{1}$$

with activation energy E_a, Vogel-Fulcher freezing temperature T_{VF}, which characterizes the temperature at which the PNRs start to freeze, i.e. become immobile, attempt frequency f_0, and Boltzmann constant k_{B}. Performing frequency-dependent measurements of $T_{\max}(f)$ in the frequency regime of 100 Hz to 1.5 MHz [see example in Fig. 4(a)], it can be demonstrated that both films show typical relaxor-type behavior in agreement with Eq. (1). By inserting a reasonable value $f_o = 4\,\text{GHz}$ for the attempt frequency, we can extract the activation energy E_a and the freezing temperature T_{VF} from the resulting Vogel-Fulcher fit. The first one describes the energy necessary for the reorientation of the polarization of the PNRs; the latter one characterizes the temperature at which the PNRs start to freeze, i.e. become immobile. Figure 4(b) exemplifies the Vogel-Fulcher analyses according to a logarithmic transformation of Eq. (1) based on measurements performed at various frequencies [Fig. 4(a)] and different electric field conditions for both $NaNbO_3$ thin films. The dash lines represent linear fits according to Eq. (1) and are used to evaluate E_a and T_{VF}.

The resulting electric field dependence of the freezing temperature T_{VF} [Fig. 5(a)] and temperature dependences of the activation energy [Fig. 5(b)] reveal a number of important information on the PNRs:

(1) First, T_{VF} hardly depends on the dc bias. For classical relaxor ferroelectrics, different field dependences have been reported. For instance, a small decrease of T_{VF} of about 4 K is reported for (Mg,Nb), doped lead titanate, whereas a small decrease of ~3 K followed by a significant increase of T_{VF} is reported for PMN for the dc field regime of 0 to $1\,\text{V}\,\mu\text{V}^{-1}$ [39,40]. However, generally, the dc field dependence of the freezing temperature is expected to be small. Therefore, it can be assumed that the size of the PNRs that contribute to the permittivity is only slightly affected by the dc field at this regime for our system.

(2) Second, however, a significant decrease of T_{VF} is observed for increasing ac amplitudes. The freezing temperature decreases by 21 and 26 K for the 63- and 27-nm-thick films, respectively, if the ac field amplitude is changed from 0.2 to $1\,\text{V}\,\mu\text{m}^{-1}$. We will use this field dependence of T_{VF} below to estimate the size of the PNRs that are active (i.e. still mobile) at the freezing temperature.

(3) Third, the magnitude of the activation energy agrees with the expected values for relaxor ferroelectrics [28,41]. Moreover, E_a decreases with temperature [Fig. 5(b)] in a linear way to zero at about 170 K. Below (see discussion of Fig. 8), we

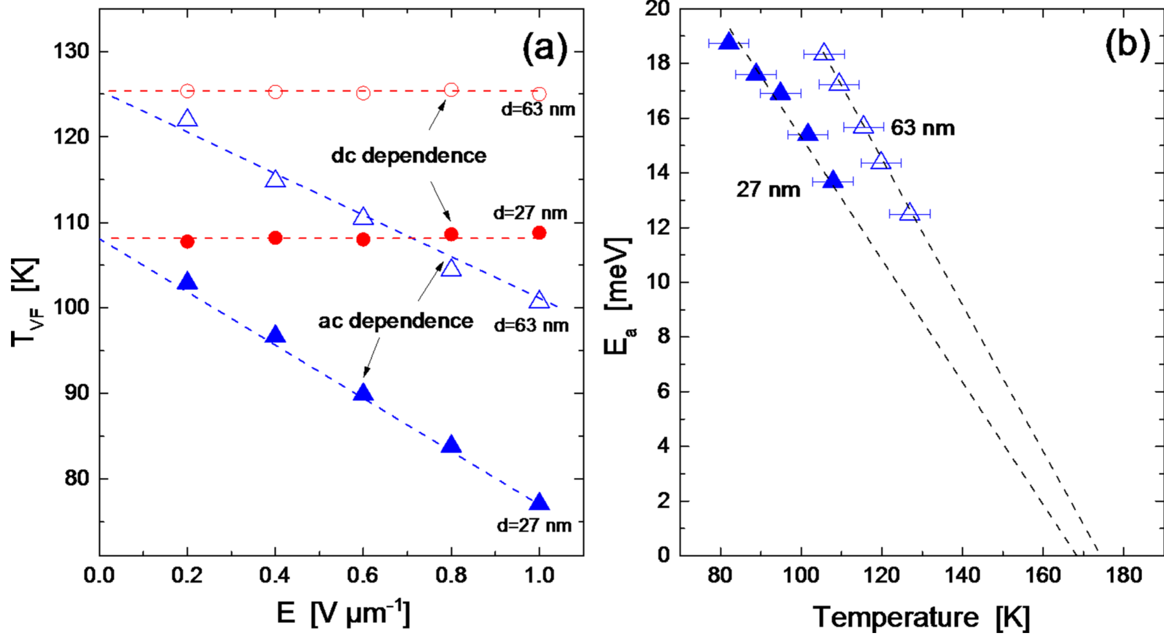

FIG. 5. (a) Freezing temperature as a function of dc (red circles) and ac (blue triangles) electric field and (b) temperature dependence of the activation energy for $NaNbO_3$ thin films with a thickness of 27 nm (solid symbols) and 63 nm (open symbols). Both parameters T_{VF} and E_a are obtained from the Vogel-Fulcher fit [Eq. (1)] as shown in Fig. 4 and using an attempt frequency of 4 GHz.

will show that, at this temperature, the irreversible contribution to the permittivity actually vanishes.

Let us first discuss the ac field dependence of the freezing temperature shown in Fig. 5(a). This dependence actually allows us to estimate the size of the active PNRs that contributes to permittivity at the freezing temperature. Comparing the change of the total energy per volume $U_e = \varepsilon'(\Delta E)^2/2$ stored by an ac electric field E in a dielectric material with the change of the thermal energy of a PNR with a volume V_{PNR} we obtain

$$V_{\mathrm{PNR}}(T_{\mathrm{VF}}) = \frac{2 \cdot k \cdot \Delta T_{\mathrm{VF}}}{\varepsilon_0 \cdot \varepsilon'(T_{\mathrm{VF}}) \cdot (\Delta E)^2}. \quad (2)$$

Inserting experimental values for ΔT_{VF} and ΔE from Fig. 5 and an estimation for the permittivity of the PNRs by using $\varepsilon'(T_{\mathrm{VF}})$ from Fig. 2, we obtain very similar values for the volume of the PNRs for both samples, i.e. from approximately 70 to 270 nm^3, which however depend on the applied ac field amplitude (see Fig. 6). Fu *et al.* reported that the PNR starts to transform its shape from spherical into elliptical at T_{VF} [6]. In order to estimate the diameter of the PNR, we assume that these PNRs are still spherical at T_{VF} in our samples. In this case, the resulting diameter of the PNRs would decrease with increasing ac field from ~8 nm at 0.2 V μm^{-1} to ~5.2 nm at 1 V mm^{-1} for both samples. The value is smaller than that reported for PFM experiments [19], however, very similar to that measured by neutron scattering [5,7] and TEM [6]. However, it should be noted that, in contrast to the microscopic data, our electronic analysis characterizes the size of the electronically active PNRs inside the ferroelectric matrix and at the freezing temperature. Furthermore, the microscopic observations refer to classical relaxor ferroelectrics, whereas our measurements are performed on strain-induced oxide thin film relaxors.

The ac electric field dependence of the PNR's size in Fig. 6 is very striking. It could be a result of the assumptions and simplifications that were used. For instance, (i) for the permittivity of the PNRs, the permittivity of the sample itself (reversible and irreversible contribution) is used, (ii) the impact of pinning on the PNRs (e.g. their polarization) is neglected, and (iii) all values represent averaged values for the size and form of the PNRs, a distribution of the PNR's size is not unlikely [42]. Nevertheless, the ac field-dependent size of the PNRs might be reasonable, since a larger driving force will lead to enhanced repolarization of the PNRs that could cause a reduction of the effective size of the polar clusters.

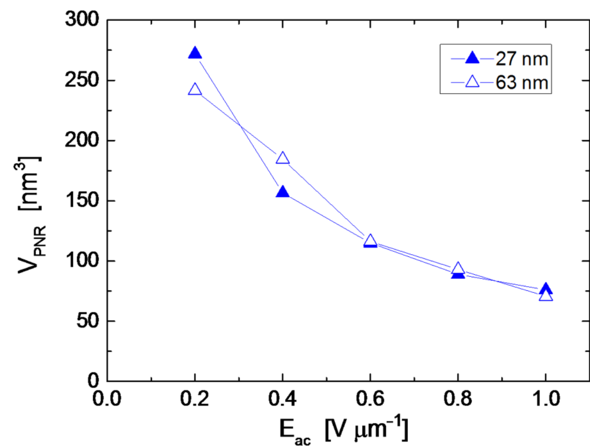

FIG. 6. Volume of PNRs that are mobile (i.e. attributing to the permittivity) at the freezing temperature as a function of applied ac electric field. The diameter is obtained via Eq. (2) assuming an idealized spherical shape for the PNRs and using the data for $\Delta T_{\mathrm{VF}}(E_{\mathrm{ac}})$ and $\varepsilon'(T_{\mathrm{VF}})$ given in Figs. 5 and 2, respectively.

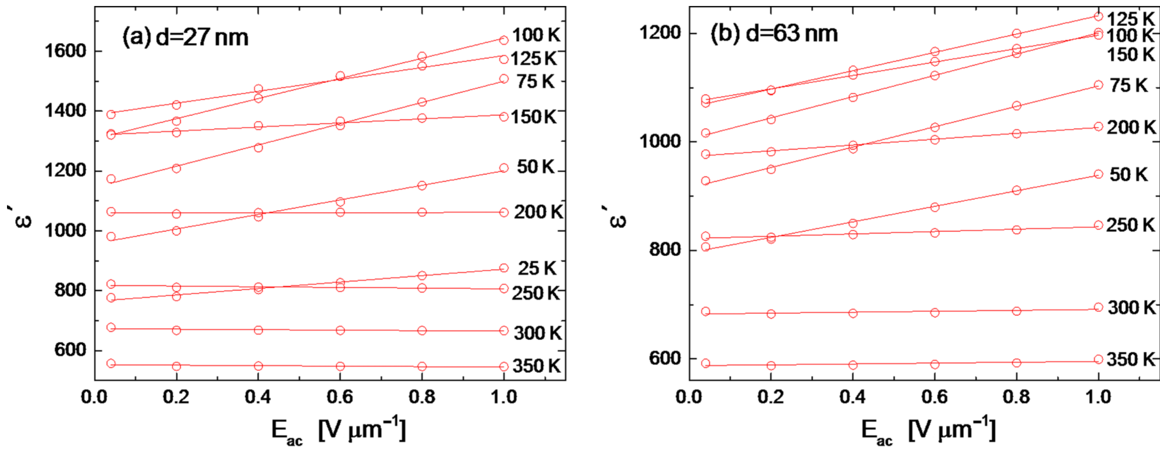

FIG. 7. Permittivity as function of the ac electric field measured at 1 MHz and different temperatures for the (a) 27- and (b) 63-nm-thick $NaNbO_3$ films, respectively. The lines represent linear fits of the data according to Eq. (3).

Finally, the contribution of the PNR to the permittivity is discussed. Figure 7 shows a set of ac field-dependent measurements of the permittivity at 1 MHz in detail. Similar measurements are performed for other frequencies. All samples exhibit a linear dependence of ε' versus E_{ac} for all temperatures and frequencies, which is a characteristic feature of hard ferroelectrics and can be described by the Rayleigh law [43]

$$\varepsilon' = \varepsilon'_{\text{init}} + \alpha E_{\text{ac}}, \tag{3}$$

where $\varepsilon'_{\text{init}}$ represents the initial (reversible) permittivity at zero electric field and α the Rayleigh coefficient that describes the irreversible properties of the polarization. In classical ferroelectrics $\varepsilon'_{\text{init}}$ represents contribution to the permittivity arising from the intrinsic lattice polarization and the reversible domain wall motions, whereas α is caused by pinning of the ferroelectric domain wall at defects [44]. In relaxor-type ferroelectrics, also the PNRs can attribute to the irreversible properties, and thus to the Rayleigh coefficient α [21,45]. Furthermore, it is known that the mobility of PNRs not only depends on the temperature, but also on the applied electric field.

For all temperatures and frequencies, the permittivity data in Fig. 7 show a linear behavior and can be fitted by Eq. (3). The resulting values for $\varepsilon'_{\text{init}}$ and α (Fig. 8) show a number of interesting features:

(1) Obviously, the initial (reversible) permittivity $\varepsilon'_{\text{init}}$ represents the permittivity expected for zero electric field. The values are slightly smaller than the experimental data obtained for finite electric fields; the temperature dependence is very similar to the one obtained for small ac fields (see Fig. 2).

(2) The Rayleigh coefficient α displays a revealing temperature dependence; it characterizes the irreversible contribution of domain walls and especially PNRs. It shows a pronounced peak at low temperature, i.e. close to the freezing temperature T_{VF}, and tends to zero at high temperature. This behavior is dominated by the presence and mobility of the PNRs [21,45]. At high temperatures, no PNRs are present. Therefore, the

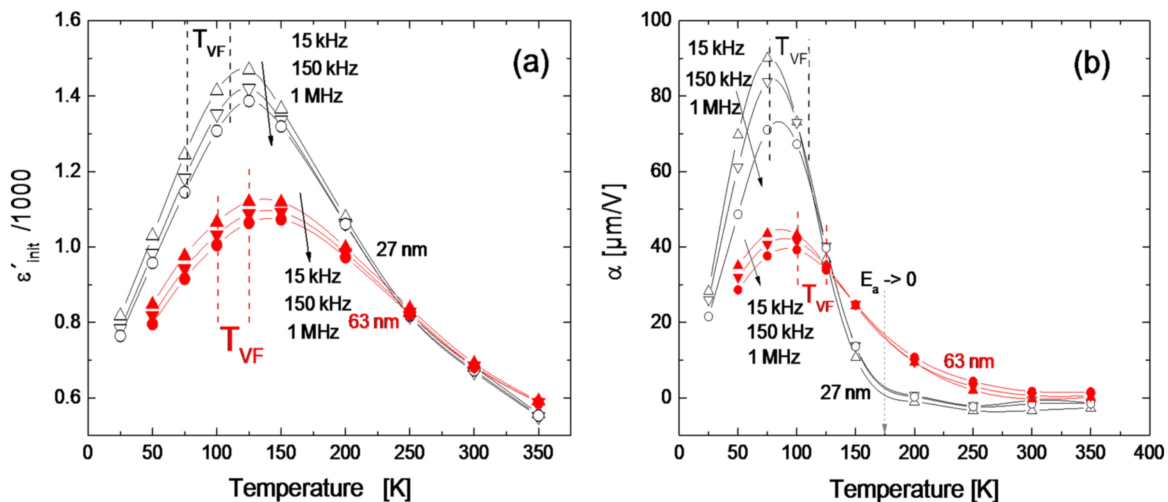

FIG. 8. (a) Initial permittivity and (b) Rayleigh parameter as a function of temperature for the $NaNbO_3$ thin films with different thicknesses, 27 nm (open symbols) and 63 nm (solid symbols), measured at frequencies 15 kHz (triangle), 150 kHz (inverted triangle), and 1 MHz (circle). The dashed lines mark the regime of freezing temperature for $E_{\text{ac}} = 1\,\text{V}\,\mu\text{m}^{-1}$ (lower temperature) and $E_{\text{ac}} = 0.048\,\text{V}\,\mu\text{m}^{-1}$ (higher temperature). The solid arrows indicate the direction of increasing frequency; the dashed arrow in (b) marks the temperature at which the activation energy extrapolates to zero (see Fig. 5).

permittivity is constant, i.e. $\alpha \approx 0$. With the transition to the relaxor state, PNRs start to form. The existence and the pinning of the PNRs lead to a field-dependent permittivity, i.e. $\alpha > 0$. With decreasing temperature, the size of the PNRs increases [7,46], and as a consequence α increases. However, at the freezing temperature, the PNRs start to become immobile; therefore, α decreases below the freezing temperature. Especially for the thinnest sample ($d = 27$ nm) with the largest strain, this behavior is very pronounced (see Fig. 8, black curves). Above $T \approx 170$ K, the Rayleigh coefficient is $\alpha \approx 0$ (i.e. no PNRs are present); only below $T \approx 170$ K, values $\alpha > 0$ are observed (PNRs are present). It should be noted that this temperature actually nicely agrees with the expected vanishing of the activation energy E_a for PNRs obtained by the linear extrapolation in Fig. 5(b). Finally, a pronounced peak at low temperature shows a maximum slightly below T_{VF}. The thicker sample (63 nm) shows a similar behavior. However, due to a larger impact of domain wall pinning that has to be expected for thicker samples, the onset of the peak at high temperature is not that sharp as observed for the thinner sample.

(3) Additional important information is given by the frequency dispersion of the data obtained for α and $\varepsilon'_{\mathrm{init}}$ in the peak regime (see measurements for different frequencies in Fig. 8). The peak position of $\alpha(T)$ and $\varepsilon'_{\mathrm{init}}$ is shifted to lower temperatures with decreasing frequency. Similar to the frequency dispersion of the permittivity, it clearly indicates, that the peak in α shows a relaxor behavior. Therefore, the reversible and also the irreversible permittivity seem to be strongly affected by the properties of the PNRs in these relaxor-type ferroelectrics.

IV. CONCLUSIONS

In conclusion, we have demonstrated that compressively strained $NaNbO_3$ films of different thicknesses that are epitaxially grown on (110) $NdGaO_3$ substrates via MOCVD technique exhibit typical relaxor-type behaviors, i.e. a broad and frequency-dispersive peak in the ε' versus T curves. The compressive in-plane strain induced by the mismatch between film and substrate leads to a shift of the phase transition temperature from 628 K for unstrained bulk $NaNbO_3$ to 125–144 K and an enhancement of the permittivity from $\varepsilon' < 500$ to ε' up to 1500 for the strained films, respectively. Both transition temperature and permittivity strongly depend on the thickness of the film. Thinner films possess a larger strain; with increasing thickness, relaxation sets in, which leads to a small increase of the transition temperature and a smaller enhancement of the permittivity at temperatures around the transition. The broadness of the transition peak and its frequency dispersion are clear indications for relaxor-type ferroelectricity. This relaxor-type behavior was examined in detail via electric field-dependent measurements of the permittivity. A small dc tunability in the form of a reduction of the permittivity of $n(1\,\mathrm{V}\,\mu\mathrm{m}^{-1}) < 7\%$ is visible in the paraelectric regime, whereas a large enhancement of the permittivity is observed if the ac field used for the measurement of the permittivity is enhanced from 0.2 to $1\,\mathrm{V}\,\mu\mathrm{m}^{-1}$. This ac field dependence reveals a lot of interesting information. First, from its frequency dispersion, we can extract the ac field dependence of the freezing temperature T_{VF} and estimations of the size of the active PNRs at the freezing temperature. According to our model, the volume of PNR varies from 70 to 270 nm^3, the resulting estimated diameter of the PNR at the freezing temperature ranges from ∼5.2 to ∼8 nm for large and small fields, respectively. These values are in agreement with literature values reported for neutron scattering experiments [5,7] and TEM measurement [6] for classical relaxor ferroelectrics. The field dependence might be explained by the size reduction caused by increasing repolarization forces. Second, the activation energy E_a of the PNRs is of the order of 10–20 meV at the freezing temperature. It decreases linearly with temperature to zero at 170–180 K, the temperature at which the irreversible contribution to the permittivity vanishes. Third, all samples show a linear ac response at all temperatures and frequencies, which is interpreted via Rayleigh law. The intrinsic or reversible polarization $\varepsilon'_{\mathrm{init}}$ shows a temperature dependence similar to that measured at small ac fields. However, the irreversible Rayleigh coefficient α is zero at high temperature, which is in agreement with the prediction of a zero activation energy, and shows a pronounced peak with a maximum slightly below T_{VF}. The position, broadness, and frequency dispersion of this peak present good indications that PNRs also play an important role in the irreversible contribution to the permittivity. In conclusion, not only the possibility to engineer the ferroelectric properties via strain, but also the prominent relaxor properties of the strained $NaNbO_3$ films represent interesting opportunities for basic research and understanding as well as possible applications of this type of ferroelectrics.

ACKNOWLEDGMENTS

The authors would like to thank A. Offenhäusser, Y. Dai, R. Kutzner, K. Greben, A. Markov, and S. Markschies for their valuable support and constructive discussion. B.C. would like to acknowledge the financial support from China Scholarship Council (CSC) under Grant No. 201206400055.

[1] See, e.g. L. E. Cross, Ferroelectrics **76**, 241 (1987), and references cited therein.

[2] See, e.g. R. Blinc, *Advanced Ferroelectricity* (Oxford University Press, New York, 2011), and references cited therein.

[3] E. Brown, C. R. Ma, J. Acharya, B. H. Ma, J. W, and J. Li, ACS Appl. Mater. Interfaces **6**, 22417 (2014).

[4] G. A. Samara, J. Phys.: Condens. Matter **15**, R367 (2003).

[5] I.-K. Jeong, T. W. Darling, J. K. Lee, Th. Proffen, R. H. Heffner, J. S. Park, K. S. Hong, W. Dmowski, and T. Egami, Phys. Rev. Lett. **94**, 147602 (2005).

[6] D. S. Fu, H. Taniguchi, M. Itoh, S.-Y. Koshihara, N. Yamamoto, and S. Mori, Phys. Rev. Lett. **103**, 207601 (2009).

[7] G. Xu, G. Shirane, J. R. D. Copley, and P. M. Gehring, Phys. Rev. B **69**, 064112 (2004).
[8] P. B. Groszewicz, H. Breitzke, R. Dittmer, E. Sapper, W. Jo, G. Buntkowsky, and J. Rödel, Phys. Rev. B **90**, 220104(R) (2014).
[9] R. Blinc, V. Laguta, and B. Zalar, Phys. Rev. Lett. **91**, 247601 (2003).
[10] G. Xu, Z. Zhong, Y. Bing, Z. G. Ye, C. Stock, and G. Shirane, Phys. Rev. B **70**, 064107 (2004).
[11] D. S. Fu, H. Taniguchi, M. Itoh, and S. Mori, *Advances in Ferroelectrics* (InTech, Rijeka, Croatia, 2012), Chap. 3.
[12] B. E. Vugmeister and M. D. Glinchuk, Rev. Mod. Phys. **62**, 993 (1990).
[13] E. V. Colla, E. Yu. Koroleva, N. M. Okuneva, and S. B. Vakhrushev, Phys. Rev. Lett. **74**, 1681 (1995).
[14] A. Levstik, Z. Kutnjak, C. Filipič, and R. Pirc, Phys. Rev. B **57**, 11204 (1998).
[15] R. Pirc and R. Blinc, Phys. Rev. B **60**, 13470 (1999).
[16] V. Bobnar, Z. Kutnjak, R. Pirc, R. Blinc, and A. Levstik, Phys. Rev. Lett. **84**, 5892 (2000).
[17] V. Westphal, W. Kleemann, and M. D. Glinchuk, Phys. Rev. Lett. **68**, 847 (1992).
[18] R. Fisch, Phys. Rev. B **67**, 094110 (2003).
[19] N. Liu, R. Dittmer, R. W. Stark, and C. Dietz, Nanoscale **7**, 11787 (2015); V. V. Shvartsman, W. Kleemann, T. Lukasiewicz, and J. Dec, Phys. Rev. B **77**, 054105 (2008); V. V. Shvartsman, W. Kleemann, J. Dec, Z. K. Xu, and S. G. Lu, J. Appl. Phys. **99**, 124111 (2006).
[20] T. Shi, L. Xie, L. Gu, and J. Zhu, Sci. Rep. **5**, 8606 (2015).
[21] S. Prosandeev, D. W. Wang, A. R. Akbarzadeh, B. Dkhil, and L. Bellaiche, Phys. Rev. Lett. **110**, 207601 (2013).
[22] H. D. Megaw, Ferroelectrics **7**, 87 (1974).
[23] Yu. I. Yuzyuk, R. A Shakhovoy, S. I. Raevskaya, I. P. Raevski, M. EI Marssi, M. G. Karkut, and P. Simon, Appl. Phys. Lett. **96**, 222904 (2010).
[24] S. K. Mishra, N. Choudhury, S. L. Chaplot, P. S. R. Krishna, and R. Mittal, Phys. Rev. B **76**, 024110 (2007).
[25] R. Wördenweber, J. Schwarzkopf, E. Hollmann, A. Duk, B. Cai, and M. Schmidbauer, Appl. Phys. Lett. **103**, 132908 (2013).
[26] R. Wördenweber, E. Hollmann, R. Kutzner, and J. Schubert, J. Appl. Phys. **102**, 044119 (2007).
[27] R. Wördenweber, J. Schubert, T. Ehlig, and E. Hollmann, J. Appl. Phys. **113**, 164103 (2013).
[28] H. W. Jang, A. Kumar, S. Denev, M. D. Biegalski, P. Maksymovych, C. W. Bark, C. T. Nelson, C. M. Folkman, S. H. Baek, N. Balke, C. M. Brooks, D. A. Tenne, D. G. Schlom, L. Q. Chen, X. Q. Pan, S. V. Kalinin, V. Gopalan, and C. B. Eom, Phys. Rev. Lett. **104**, 197601 (2010).
[29] B. Cai, J. Schwarzkopf, E. Hollmann, M, Schmidbauer, M. O. Abdel-Hamed, and R. Wördenweber, J. Appl. Phys. **115**, 224103 (2014).
[30] R. Dirsyte, J. Schwarzkopf, G. Wagner, J. Lienemann, M. Busch, H. Winter, and R. Fornari, Appl. Surf. Sci. **255**, 8685 (2009).
[31] J. Schwarzkopf, M. Schmidbauer, T. Remmele, A. Duk, A. Kwasniewski, S. Bin Anooz, A. Devi, and R. Fornari, J. Appl. Crystallogr. **45**, 1015 (2012).
[32] A. Vailionis, H. Boschker, W. Siemons, E. P. Houwman, D. H. A. Blank, G. Rijnders, and G. Koster, Phys. Rev. B **83**, 064101 (2011).
[33] O. G. Vendik, S. P. Zubko, and M. A. Nikol'skii, Tech. Phys. **44**, 349 (1999); O. G. Vendik and M. A. Nikol'skii, *ibid.* **46**, 112 (2001).
[34] S. S. Gevorgian, T. Martinsson, P. L. Linner, and E. L. Kollberg, IEEE Trans. Microwave Theory Tech. **44**, 896 (1996).
[35] E. Chen and S. Y. Chou, IEEE Trans. Microwave Theory Tech. **45**, 939 (1997).
[36] G. Shirane, R. Newnham, and R. Pepinsky, Phys. Rev. **96**, 581 (1954).
[37] S. Wada, H. Adachi, H. Kakemoto, H. Chazono, Y. Mizuno, H. Kishi, and T. Tsurumi, J. Mater. Res. **17**, 456 (2002).
[38] H. Vogel, Physikalische Zeitschrift **22**, 645 (1921); G. S. Fulcher, J. Am. Ceram. Soc. **8**, 339 (1925).
[39] Z. Kighelman, D. Damjanovic, and N. Setter, J. Appl. Phys. **90**, 4682 (2001).
[40] D. Viehland, S. J. Jang, L. E. Cross, and M. Wuttig, J. Appl. Phys. **69**, 414 (1991).
[41] D. Viehland, S. J. Jang, L. E. Cross, and M. Wuttig, J. Appl. Phys. **68**, 2916 (1990).
[42] R. Pirc and R. Blinc, Phys. Rev. B **76**, 020101(R) (2007).
[43] L. Rayleigh, Philos. Mag. **23**, 225 (1887); D. Jiles, *Introduction to Magnetism and Magnetic Materials* (Chapman and Hall, London, 1991), pp. 85–175.
[44] D. V. Taylor and D. Damjanovic, J. Appl. Phys. **82**, 1973 (1997).
[45] B. H. Ma, Z. Q. Hu, S. S. Liu, S. Tong, M. Narayanan, R. E. Koritala, and U. Balachandran, Appl. Phys. Lett. **102**, 202901 (2013).
[46] Y. P. Shi and A.K. Soh, Appl. Phys. Lett. **99**, 092908 (2011).